Journal of Structural Geology 30 (2008) 1126–1137

Contents lists available at ScienceDirect

Journal of Structural Geology

journal homepage: www.elsevier.com/locate/jsg

Confluence and intersection of interacting conjugate faults: A new concept based on analogue experiments

H.-U. Schwarz [a,*], F.-W. Kilfitt [b]

[a] Institut für Geologie, Mineralogie und Geophysik, Ruhr-Universität Bochum, Universitaetsstrasse, D-44801 Bochum, Germany
[b] Institut für Geotechnik Dr. J. Zierfas, D-65556 Limburg, Germany

ARTICLE INFO

Article history:
Received 11 January 2008
Received in revised form 25 April 2008
Accepted 15 May 2008
Available online 21 May 2008

Keywords:
Conjugate faults
Fault interaction
Fault confluence and intersection
Activity cycles

ABSTRACT

Examination of the interaction area of conjugate faults yields evidence of a yet unknown structural pattern. Analogue experiments revealed the evolution of this pattern during the interaction process. A fault propagating towards the highly active section of another conjugate fault becomes increasingly deflected towards the obtuse angle side of the conjugate system while approaching until joining it. During this process, the tip of the curved propagating fault retains its shear sense until immediately before joining with the highly active fault—a process called "confluence" in this report. Under constant remote stress, the deflected fault now becomes dominant. A fault branch splits off at the point where deflection commences, propagating straight ahead of the original direction, and may dissect the former master fault. Alternating activity at both of the faults finally produces the known intersection patterns. Further studies of the proposed concept on natural examples are recommended due to the close geometric similarity of the evolutionary structural stages and natural fault patterns.

1. Introduction

Study of conjugate faults yields evidence of their interaction and the dynamic processes governing growth of the fault sets and displacement along them. The key question has been investigated in detail: what happens in the region of intersection? Watterson et al. (1998) distinguish between three methods of establishing the volume balance: (a) ductile thinning by inter-grain slip, (b) pressure solution, and (c) multiple cross-cutting faulting. Another mode of volume accommodation is mass transport toward the surface resulting in flower structures. In this study, we describe an additional kinematic process and its structural features of interacting conjugate faults within the intersection region.

Most of the intersections of natural faults present sharp-cut junctions with or without displaced sections or display a strongly fragmented damage zone. The literature on conjugate faults generally recognizes these types. Surprisingly often, however, the region of potential or existing intersection of conjugate faults reveals a curved link between the faults on the obtuse angle side (Fig. 1).

The lack of a detailed description of such curved links (excluding short notes by Anderson, 1951, p. 53 ff. and Reches, 1988, p. 147) or even of an explanation for such a geometric feature induced us to perform analogue experiments and to examine the generation and kinematic function of these curved links and related structures. Their frequent occurrence in nature at a wide range of scales makes them appear the specific result of an interaction process at conjugate faults producing a sequence of characteristic geometric patterns.

We differentiate between four main types (Fig. 2). A small fault 2 propagating towards a pre-existing fault 1 becomes increasingly deflected into the shear direction of fault 1 (Fig. 2a,b). This deflection process results in a curved linkage between the conjugate faults, comparable with the joining of a confluent river with the main river (Fig. 2b). We call this type and process "confluence". The occurrence of an additional fault 2 branch propagating in a straight direction towards fault 1 marks a new structural development (Fig. 2c), which may be followed by the intersection and displacement of fault 1 (Fig. 2d).

Although the intersection process is well known (Watterson et al., 1998: cross-cutting faulting; Ferrill et al., 2000: crossing conjugate faulting), it has seldom been considered part of a larger evolutionary process (e.g. Davatzes and Aydin, 2003; Flodin and Aydin, 2004: sequential jointing and shearing). Therefore, it appears appropriate to focus on the development of the structure types of Fig. 2 and to integrate them into the entire interaction process. Under this aspect, we restrict the term "intersection" to the cross-cutting patterns of type d of Fig. 2.

The kinematic principle of interacting faults can best be studied using single fault elements. However, the ubiquity of the structures

* Corresponding author. Tel.: +49 2302 21303.
E-mail address: hans-ulrich.schwarz@rub.de (H.-U. Schwarz).

0191-8141/$ – see front matter © 2008 Elsevier Ltd. All rights reserved.
doi:10.1016/j.jsg.2008.05.005

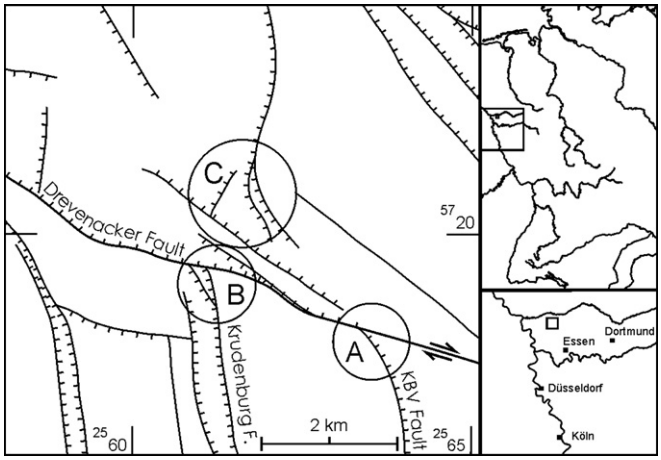

Fig. 1. Fault pattern around the Drevenacker fault in the northern Ruhr district, Germany with three examples of curved links between conjugate fault sets (A, B, C). Simplified redrawn from Wolf (1988), plate 1.

of interest and the problem of their fractal order in any material and on any scale suggest that shear zones should also be included in the investigation. In this report, we use the term "shear zone" for a zone of synthetic and antithetic fault sets organized into domains or as a chain of en echelon faults, including their damage zones. Shear zones and faults can be constituents of a conjugate system with equal kinematic functions.

2. Analogue experiments

2.1. Equipment

Three shear devices designed for easily deformable materials have been used:

(1) The **Bochum deformation stage (BDS)** (Figs. 3a and 4) has been constructed for homogeneous strain under axial, rhombic (pure shear), monoclinic (simple shear), triclinic or combined symmetry conditions. Here, it has been used under equal area conditions. The stress is exclusively induced into the material (Table 1) by frictional contact to a thin latex cloth, which rests slightly pre-stretched on 121 square metal plates. Every one of them is moved in exactly the same manner by translation and/or rotation. In this way, a homogenous distribution of strain is achieved over a clay cake area of about 50 × 50 cm. The appropriate thickness of the material cake ranges from 2 cm to 8 cm. The driving control enables strain rates from $1.9 \times 10^{-3}\,s^{-1}$ to $4 \times 10^{-6}\,s^{-1}$. Variable strain rates are possible if desired. The range of motion of each metal block restricts the total strain. Under pure shear conditions a maximum strain ratio of $R_s = 4$ can be reached; under simple shear conditions the maximum shear value is $\gamma = 3.5$. For further details of the construction see Hoeppener et al. (1968, 1969).

(2) The **parallel dislocation stage (PDS)** (Fig. 3b) allows displacement of one half of a table plate in any direction parallel to a main shear plane, for which the angle of inclination can be varied from 90° to a very low dip. The total size of the table is

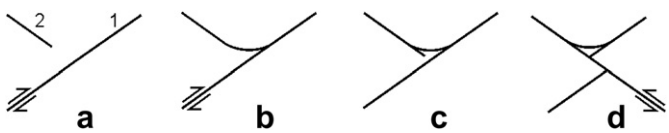

Fig. 2. Typical patterns of a conjugate fault system. (a) Simple system consisting of a dextral fault 1 and a sinistral fault 2 growing towards fault 1. (b) Curved linkage of both faults—called "confluence" in this report. (c) Fault 2 branch propagating in straight direction. (d) Intersection of fault 1 by fault 2.

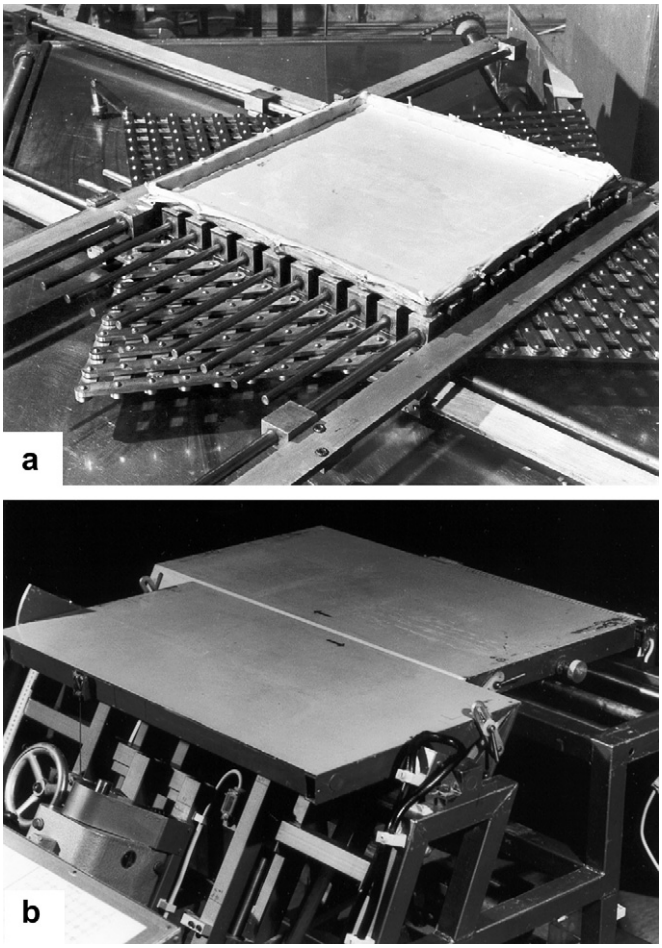

Fig. 3. (a) Material trough of the Bochum deformation stage (BDS) at a square position. A rubber cloth rests upon 121 square metal plates connected to each other by two sets of rods and a scissor grid. This construction can be driven by up to three spindles over two double sets of long metal bars, so that these rotate or move towards or away from each other. (b) Parallel dislocation stage (PDS). One plate can be moved horizontally, the other vertically along an inclinable shear plane. The material rests freely upon both plates.

100 × 100 cm. The material cake can be up to 30 cm thick, but in general, thicknesses of 5–8 cm have been used. The achievable strain rates are similar to those of the BDS. A horizontal table displacement of up to 50 cm is possible, corresponding to a shear value of $\gamma = 6.25$ at an assumed shear zone width of 16 cm. The material cake rests freely on fixed grinding paper on the table without any lateral support. Amongst other things, this table is suitable for simple shear studies of the early shear zone development, because no additional compressive or tensional stress is applied. This restriction appears acceptable, as a broad variety of structural features of a shear zone is generated including those that are generally thought to be due to transpressive forces (e.g. transpression folds, flower structures), or transtensional forces (e.g. depressions, pull-apart structures). Another advantage is the restriction to only one master shear zone including sub-shear zones down to several fractal orders.

(3) A **micro-shear set (MSS)** has been used as an auxiliary device for observations of the development of microstructures under a stereomicroscope. It consists of small hand-driven plastic plates with a thin clay bed spread on them. One plate is fixed on the table, the other slowly moved by hand. Although this simple technique does not enable adjustment of the shear rate, one can examine all details of the structural development. Such experiments can be repeated quickly. The resulting data sets have not been recorded.

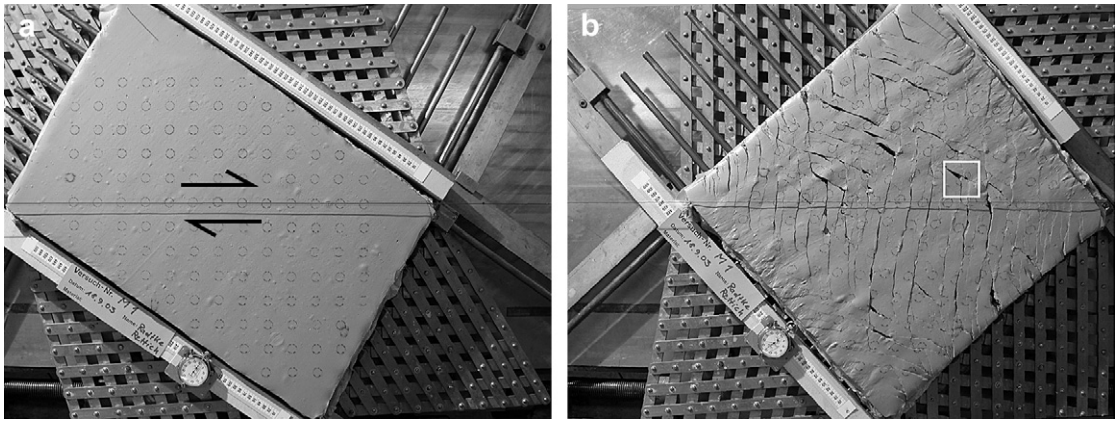

Fig. 4. Start (a) and end (b) configuration of simple shear experiment M1 (cf. Table 1) under equal area conditions (area (a) = area (b)) on the Bochum deformation stage. Black line: orientation line. Confluence and intersection occur at the domain borders of the parquetry pattern. Boxed area (b) is the site of detailed drawings of Fig. 5, actually that of Fig. 5h.

2.2. Material and preparation of the test blocks

Clay mud with a 30% water content was used (ground industrial clay: >20 μm: 11%, 20–6.3 μm: 24%, 6.3–2 μm: 20%, <2 μm: 44%; X-ray analysis of fraction <2 μm: 42% illite, 30% quartz, 25% kaolinite, 3% mixed layers including smectite). Special care was taken to obtain a homogeneous cake with as few air bubbles as possible.

Due to the platy nature of the clay minerals, it is impossible to produce a smooth surface of the clay cake without generation of a thin anisotropic zone of slightly inclined and parallel-arranged clay platelets (Weber, 1976). The strike direction of these platelets determines if or how faults will develop (Hoeppener et al., 1978; Hoeppener and Schwarz, 1980). Thus, a direction of smoothening of the clay cake surface that would achieve a well-balanced frequency distribution of both of the conjugate fault sets was chosen.

Instead of marker imprints on the clay surface, which would reselect the site of the first ruptures, fine grinding powder (carborundum) was sprinkled through a template with fine holes to produce lines or circles (Fig. 4a). An additional black string was fixed over each test block as an orientation marker to show the position of either the table shear plane (at PDS) or the orientation of the general shear direction (at BDS). All angular data refer to this line and are measured in the direction of the shear sense.

Each experiment has been documented by photographs taken at regular intervals (generally 5–20 min). In two experiments (M1,V31), very short intervals (30 s) were used to examine all changes in shear activity (Table 1).

2.3. Experimental observations

2.3.1. General remarks

In compliance with the construction of the devices used, all experiments were performed under strain-induced conditions producing stress within the clay material. In nature, the conditions are reversed. Therefore, we prefer fabric-orientated studies (cf. Tikoff and Wojtal, 1999). It was not possible to install stress sensors within the clay cake without considerable disturbance of the fabric development. Therefore, two BDS experiments (9 stages of each) were used for strain measurements on deformed circle markers (6 mm in diameter, 10 mm spacing) to provide the database of contour maps of strain and strain orientation.

Their analyses, however, did not reveal the expected coherence with the fault pattern developed. The rotation of the long axis of the marker ellipses (maximum of over 30°) within apparently unfaulted blocks is not uniform. At some sites, intervals of rotation reversal even occurred. Furthermore, there are areas where the maximum R_s value is accompanied by the minimum angle of rotation and vice versa. However, at many sites near faults or in block centres, both values are in accordance with each other. In summary, the curves of strain and strain orientation over all stages indicate an oscillating trend. There appears to be a principal mechanism in action, which is not only simulated by measurement errors and too coarse dimensioning of the marker objects. We would like to present the structural results of the induced deformation before discussing these effects in a separate study.

Table 1
General data of selected simple shear experiments

Serial number of experiment	M1	K19	K27	V31	V30
	Figs. 4, 5	Fig. 6	Fig. 10	Figs. 7, 8	Fig. 9
Deformation stage[a]	BDS	BDS	BDS	PDS	PDS
Material[a]	Clay/water	Clay/water	Clay/water	Clay/water	Clay/water
Water content	32.4%	30.0%	29,0%	31.4%	30.1%
Block size l/w/h (cm)					
initial:	62.1/40.0/4.2	68/38.5/3.2	66/39/3.2		
final:	47.8/53.0/4.2	49/51.5/3.2	51/50/3.2	95/44/6.5	86/60/10.2
Angle of anisotropy[b]	135°	135°	135°	135°	22°
Marker type; size (cm)	Circles: 1.5 cm	Grid: 1 cm	Circles: 0.5 cm	Circles:1.5 cm	Grid: 2 cm
Shear sense	Dextral	Sinistral	Dextral	Dextral	Dextral
Max. shear zone width (cm)	Entire surface	Entire surface	Entire surface	7.0	Inhomogeneous
Max. amount of shear (γ)	0.5531	0.6364	0.5361	2.8571	1.2538
Mean shear rate ($\gamma\ s^{-1}$)	4.045×10^{-5}	5.7333×10^{-5}	4.200×10^{-5}	7.1073×10^{-4}	1.1609×10^{-4}
Duration of experiment	224 min	185 min	215 min	67 min	180 min
Number of photographs	400	16	10	110	30
Interval of photo shots	30 s	Irregular	20 min	30 s	5 min

[a] For description see text.
[b] Strike direction of clay platelets related to applied shear sense.

The available data set (mainly photographs) is based on 81 shear zone experiments using the PDS and 26 equal area and homogeneous strain experiments using the BDS. Five experiments have been selected to illustrate evolution and variety of confluence and intersection structures (Table 1).

2.3.2. BDS experiments

Fig. 4 displays an overview of the initial and final stage of experiment M1 (Table 1). Domains of synthetic and antithetic faults have developed. At late deformation stages, synthetic faults are slightly opened (black shadows), whereas antithetic faults appear compressed; this is due to strong internal rotation. One can detect curved fault terminations at the domain borders, which are of special interest to us.

The fault development within the boxed area in Fig. 4b has been traced and redrawn from photographs of eight selected stages (Fig. 5a–h). The increasing number and length of synthetic faults up to stage (d) is followed by inactivation and obliteration of some of them (Fig. 5e–f), whereas others become enhanced, e.g. the synthetic fault within the deformed marker circle (Fig. 5e–h). In contrast, the increase of the antithetic elements starts significantly later (Fig. 5c–f). The opening of the central synthetic fault (Fig. 5f–h) coincides with enhanced shearing along the antithetic faults (documented by displacements of marker sections). Stages (g) and (h) are characterized by the additional occurrence of PDZ (principal displacement zone) elements. The black shadow of the antithetic fault on stage (h) marks compression and some thrusting. The angle of internal rotation of the oldest antithetic faults ranges to over 20°, whereas that of synthetic faults ranges to about 10°. One should note that propagated new fault sections occur under exactly the angle measured at early stages (Fig. 5a,b). This results in slightly curved faults at late stages (Fig. 5g,h). Many sites, e.g. in the area of the deformed marker circle or near the lower left corners of Fig. 5, display early stages (Fig. 5b–d) of confluence bows followed by branching in a straight ahead extension exactly at the beginning of the confluence bow (stages d–f) or even cross-cutting in late stages (Fig. 5f–h).

For better comprehension of the displacement processes along synthetic and antithetic faults, a small part of the surface pattern of experiment K19 (Table 1) has been examined by detailed slip measurements at six selected stages (Fig. 6, series on left side). The stages were selected for their characteristic evolutionary fault pattern displaying confluence and interference, mainly documented by the antithetic fault. The stages are separated by different time intervals. On the right-hand side, circles of diverse diameters indicate the amount of displacement at the circle centre. Black circles mark distinct displacement activity at the time and point of observation, whereas white circles indicate no or little activity. Several activity changes are discernible when considering only the elements with high activity: from synthetic elements (stage a) to antithetic elements (stages c,d) and back to synthetic elements (stages e, f). These activity changes correspond to the formation of new structural features. In accordance with the observations on stages (b) and (c) of Fig. 5, the high activity of the synthetic faults displayed in Fig. 6a correlates with the formation of the confluence bows at either end of the growing antithetic fault (stages a, b). The subsequent dominance of the antithetic fault (stage d) is structurally documented by its straight ahead branching and intersection of the lowermost synthetic fault. Finally, the synthetic faults dominate yet again, as shown by intersection and displacement of the antithetic fault (stages e, f). This behaviour is discussed below.

2.3.3. PDS experiments

Fig. 7 presents the final stage of the PDS experiment V31 (Table 1) showing a typical Riedel pattern of a broad shear zone consisting of a chain of domains with synthetic or antithetic fault elements and transpression folds. The latter were generated before the fault pattern occurred, but they have been enhanced in later stages of the shear zone evolution. The antithetic elements display a sigmoidal shape (boxed area of Fig. 7 and on the right-hand side thereof) due to strong internal rotation of their older central sections, whereas the younger outer tips are less rotated or unrotated. The synthetic elements appear opened at their central sections. A closer look at these central sections reveals edges parallel to the

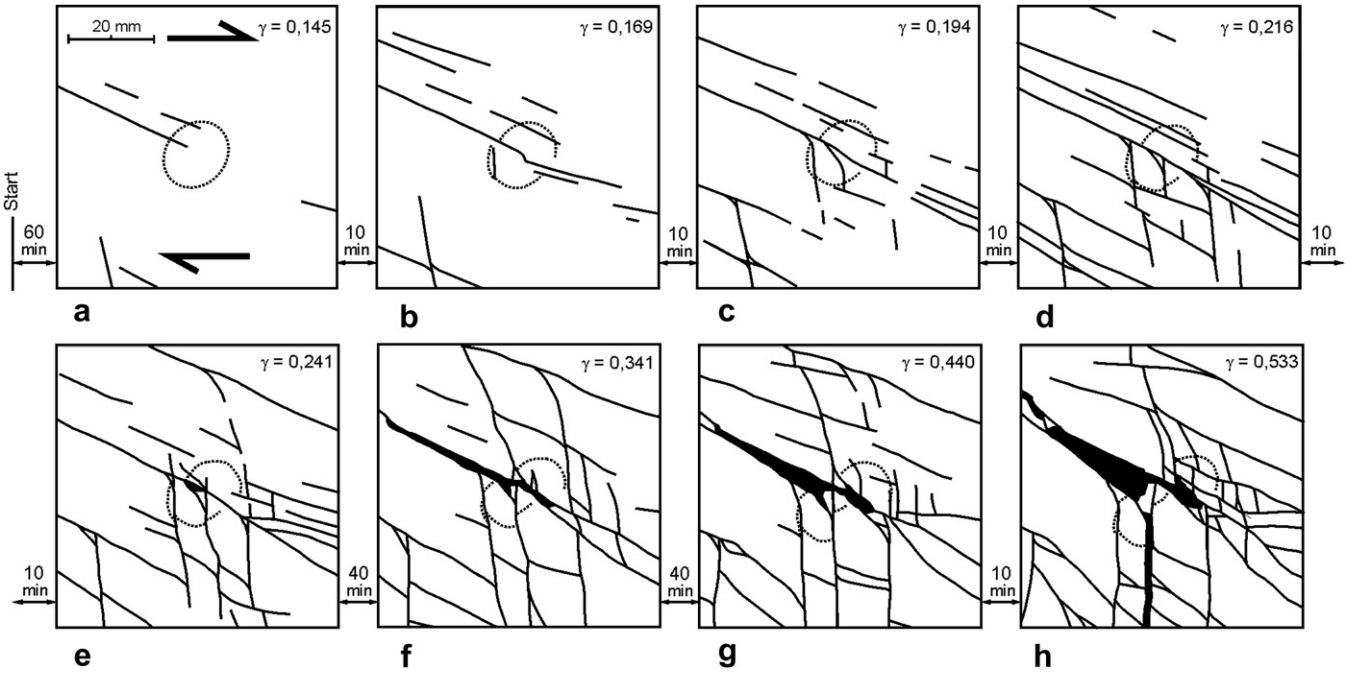

Fig. 5. Selected stages of experiment M1 with long time intervals (compared to those of Fig. 8). Note the changing fault propagation and the displacement progress at the primary circle marker (dotted). For detailed description, see text. Black: opened synthetic fault and shadow of a thrusted antithetic fault.

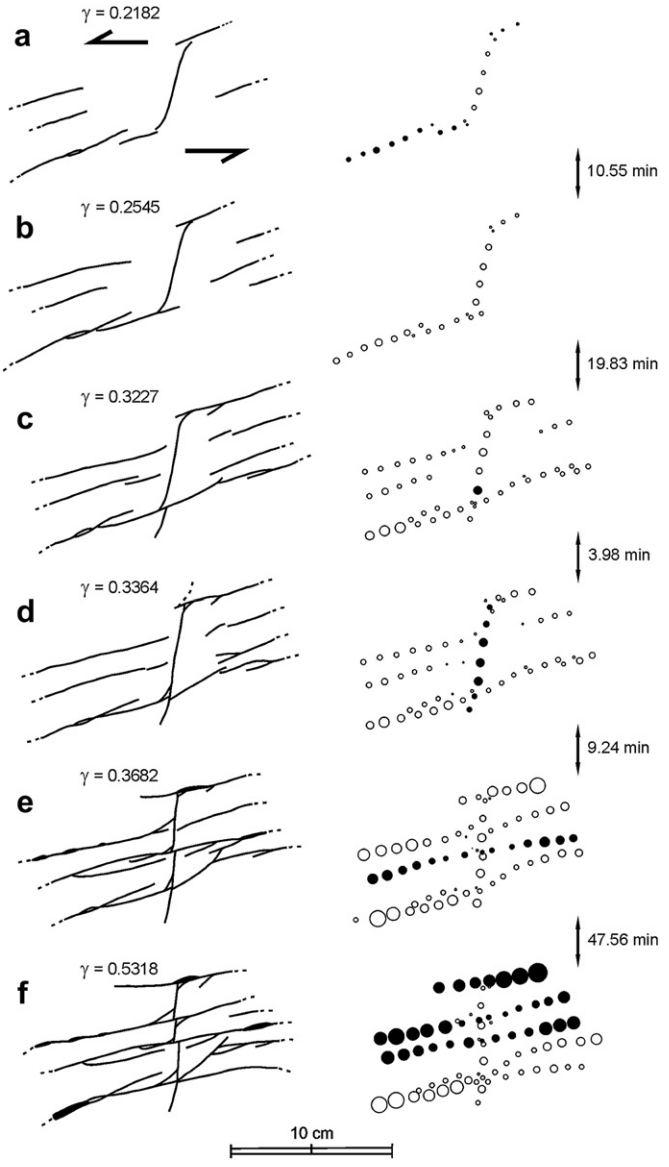

Fig. 6. Documentation of propagation and displacement activity of synthetic and antithetic elements at characteristic stages. Simple shear experiment K19 (cf. Table 1) with the Bochum deformation stage. Circle diameters indicate total amount of displacement achieved at that stage. Filled circles: actual activity of the element. Open circles: inactivity. Dotted fault terminations: fault continues outside the drawing. Note the general activity change from synthetic (a) to antithetic (c, d) and back to synthetic faults (e, f).

orientation line and proves them to be PDZ features developed during a late stage of the shear zone evolution.

The best insight into the fault interaction processes is provided by a short-interval documentation of experiment V31 with photo shot intervals of 30 s (Table 1). The boxed area on Fig. 7 has been selected for a detailed examination of the fault pattern evolution (Fig. 8). For a better overview, the time intervals between the ten stages depicted have been slightly enlarged without omission of any important steps (excluding final stage (j), which corresponds to Fig. 7).

Among the vast number of fault interaction sites studied, only one small but typical site is highlighted here (circled in Fig. 8). The interaction process starts with the growth of the antithetic fault towards the centre of a synthetic en echelon segment (Fig. 8a,b). One minute later (Fig. 8c), the antithetic fault has propagated in a curved manner and joined with the small synthetic fault near the margin of the circle on the right-hand side. This is what we call "confluence". In the interim, the initially separated synthetic segments (Fig. 8a) became linked to a continuous fault zone throughout the circle area (Fig. 8c,d). The occurrence of tiny antithetic elements within this synthetic fault zone indicates that this process was not continuous, but must have been interrupted by shorter periods of antithetic fault activity than revealed with the 30 s intervals. Stage (d) shows a split-off of a new antithetic fault branch along the original strike direction of the antithetic fault at the very beginning of its deflection. This branch grows and gets into contact with the synthetic fault within the next 2 min (Fig. 8e), and after a period of synthetic shear (Fig. 8f) it dissects the synthetic fault and displaces it (Fig. 8g,h). Small linkage fractures enable further displacement over the fault steps (Fig. 8i,j). Finally, the dextral shear activity dominates within the entire shear zone and the antithetic elements become dissected and deformed by internal rotation and compression (see arrow on stage j).

The enlarged section of the central part of the shear zone of experiment V30 (Fig. 9) reveals further details, which may be indicative of the process responsible for the formation of confluence structures. A network of conjugate faults shows all types of interaction structures (as defined by Fig. 2) on the background of highly rotated and faulted grid lines. Confluence bows have developed at nearly every intersection site. In view of the interior of the blocks enclosed by the conjugate faults, it is possible to discern systems of micro-faults. These are mainly parallel to synthetic boundary faults and are less than 1 mm apart. The almost orthogonal grid lines to these systems appear to be composed of tiny offset increments. A rotated straight grid line results if they are integrated. Moreover, the formation of mode I splay faults at the tip of the antithetic fault near the centre of the Fig. 9 was also observed. Their role will be discussed later.

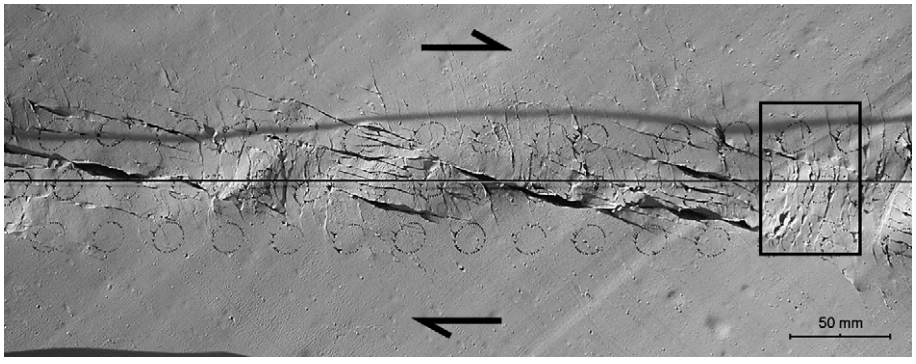

Fig. 7. Final stage of simple shear experiment V31 (cf. Table 1) on the parallel dislocation stage with transpression folds and domains of synthetic and antithetic fault sets. Synthetic faults are partly open (black), antithetic faults are compressed and strongly rotated in the central sections. Note thrusting of the faulted blocks with their acute angle corner. The boxed area is the site of detailed drawings of Fig. 8, actually that of Fig. 8j. Black line: position of the table shear plane. Deformed markers: circles of originally 15 mm in diameter.

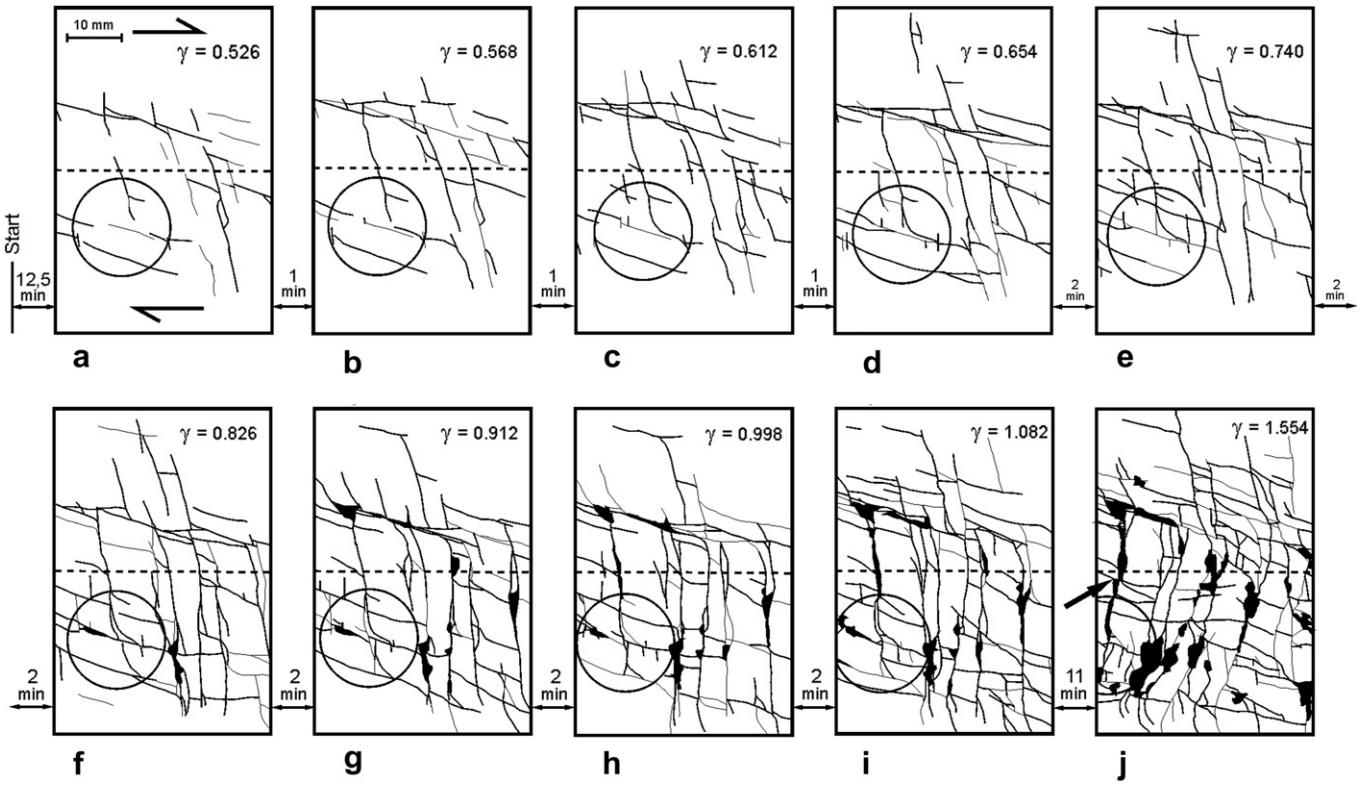

Fig. 8. Selected stages of experiment V31. Note the short, but varying time intervals. Circle is to direct viewers' attention to structural development of confluence and intersection features including alternating propagation activity of the conjugate fault sets. Arrow (j) marks displacement along a synthetic and a new PDZ element as example for the final dominant activity. For detailed description, see text. Black: shadow areas due to opened synthetic or thrusted antithetic faults. Dashed line: position of the table shear plane.

2.4. Structural development of the observed patterns

2.4.1. Structural features

The observations of the structural development of conjugate faults in all shear experiments performed in our laboratory correspond well with each other. To avoid confusion, we use the label number 1 for the first fault discernible in the field of interest, and number 2 for the next conjugate fault discernible.

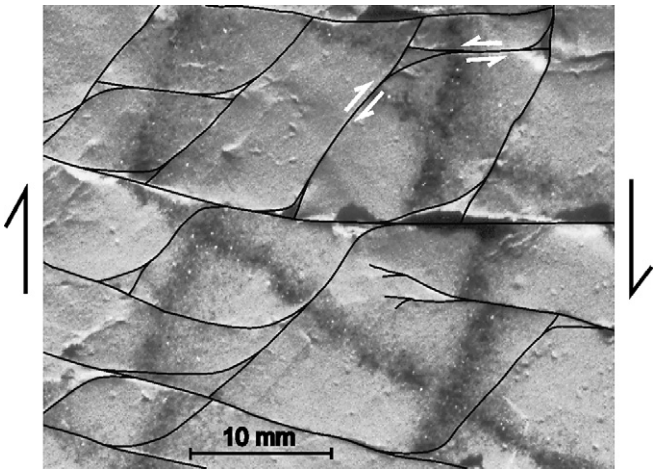

Fig. 9. Enlarged section of the final stage of simple shear experiment V30 (cf. Table 1) on the parallel dislocation stage. The orthogonal marker grid has been strongly rotated and faulted. Most fault traces have been redrawn. Each fault interaction site displays a confluence bow and (mostly) intersection features (e.g., fault branches, displaced fault intersections). Note two small splay faults near the centre of the picture and the dense system of mainly synthetic deformation bands (not redrawn).

The deformational behaviour of the unfaulted clay cake at an early stage was omitted in the preceding text, because detailed descriptions thereof have been presented by Hoeppener et al., 1969, (figures 7 and 13), Kalthoff (1970), and Schrader (1970). We also observed sets of either synthetic or antithetic deformation bands (lines of plastic flow defined by microscopic offset within the size of the clay aggregates without discernible ruptures; Schrader, 1970) forming domains of each set with some interfingering at the domain borders. Later on, single faults occur within these domains directly parallel to the prevailing deformation band set. These faults propagate and dominate the macroscopic deformational pattern. Some of our observations (Fig. 9) suggest that the early deformation bands might later mutate to micro-faults remaining active at a lower level in addition to the higher shear activity of the macroscopic faults.

The most conspicuous element of the commencing interaction process is the confluence bow (Fig. 2b). It always grows as a curve from the tip of fault 2 in shear direction of the conjugate fault 1 until joining it (Figs. 1A, 5a–c, 6a, 8c). When such curves were slightly magnified, we sometimes observed an en echelon pattern, where each small segment that occurred, turned somewhat more into the curve direction than the preceding one. Wherever one of these segments cuts a marker, the offset corresponds to the shear sense of fault 2, albeit with a decreasing amount, towards fault 1. Generally, the last segment before joining with fault 1 is thrust-faulted with the acute angle corner of the block between fault 1 and 2 (Figs. 7, 9, 10). On the other hand, this segment sometimes coincides with a synthetic en echelon element of fault 1, which has a reversed shear sense and is somewhat longer than a segment of the confluence bow. It appears as if the reversal of the shear sense of the confluence bow to that of fault 1 does not occur until entering the shear zone of fault 1. In our experiments, these fault 1 shear zones are relatively narrow with maximum widths of 5 mm

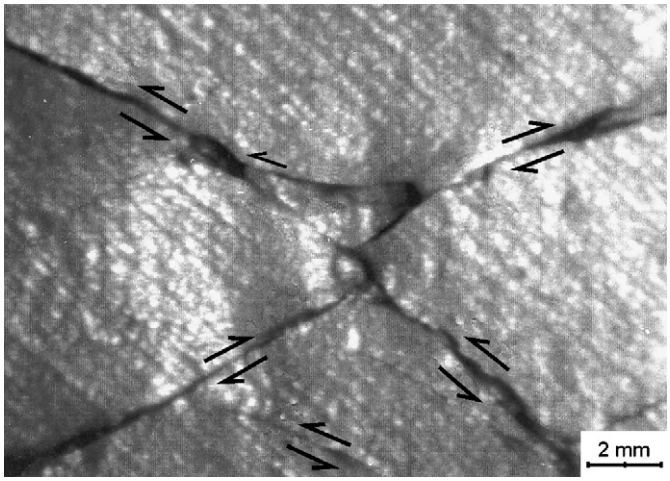

Fig. 10. Typical conjugate fault system with intersection pattern (simple shear experiment K 27, cf. Table 1). Confluence bow and displaced intersection of the primary dextral fault indicate multiple activity changes of the elements. For detailed interpretation, see Fig. 11. Due to the magnification, the clay surface appears grained and grooved, which has been caused by smoothening of the clay cake containing a portion of not fully homogenized clay aggregates.

(measured by the spread of en echelon segments). Adjacent damage zones were detected at some segments, but they are difficult to identify. Therefore, they are subsumed into the shear zone width. In contrast, the deflection of fault 2 starts at a distance from fault 1 (up to 2 cm), which is about four times greater than the shear zone width.

According to our observations we have to define another structural element, namely the straight ahead propagated section of fault 2 (Figs. 1B,C, 5d–g, 6d, 8d,e, 9). As second element of the interaction process on that fault, we call it "confluence branch". Its generation implies a revitalization of fault 2. All of the other features of interacting conjugate faults are known in the literature: intersection and displacement of either faults including formation of linkage faults (Figs. 5g,h, 8g–j; Horsfield, 1980; Reches, 1988; Lamouroux et al., 1991; Nicol et al., 1995; Watterson et al., 1998).

The interaction process of conjugate faults as part of a greater shear zone (PDS experiments) ends with the final dominance of movements along synthetic faults, the formation of gaps along them, or newly developed PDZ elements.

At this point, it appears appropriate to emphasize that theoretically confluence may develop on both sides of fault 1, although generally only one-sided confluence is generated. A symmetric structure forms if two originally separated type 2 faults propagate towards fault 1 from either side thereof and each of them creates a confluence bow. This needs not necessarily happen at the same time. Later confluence branches may join together, dissecting fault 1. Such an intersection pattern is shown in Figs. 10 and 11i (BDS experiment K27). Only the final fault pattern has been photographed, thus stages (a)–(h) of Fig. 11 have to be considered a logic reconstruction based on observations of the development of such experimental patterns.

2.4.2. Alternating shear activity

The observed structural evolution of confluence und intersection structures (Figs. 5, 8) and direct slip measurements (Fig. 6) reveal an alternating growth and shear activity at both of the conjugate fault sets. This is shown in Fig. 11, where at each stage the growth of a new fault element is directly correlated with the shear dominance of only one of the two fault sets.

The confluence bows of the antithetic fault on Fig. 6 suggest that even before stage (a) at least two activity periods must have occurred here. Similar inferences can be drawn from the study of the synthetic fault set: the occurrence of new synthetic elements at stages where only the antithetic fault is marked as active, require additional stages of synthetic activity periods between stages (c) and (e).

The results of experiment V31 (Fig. 8) with very short photograph intervals suggest relatively short activity periods of less than 1 min. On the other hand, stage (c) of Fig. 11 seems to imply that the confluence bows (3) are formed during one dextral activity period (period of dextral shear). Likewise, the details of Fig. 8a–c support the idea of one dextral activity cycle during which the confluence bow developed. Here, however, the occurrence of tiny antithetic elements indicates a very short interruption of the dextral activity by a sinistral one. Long or irregular time intervals between the stages documented in Figs. 5, 6 and 8d–j therefore seem to include more activity changes than the development of the main structural features suggests at first glance. Such a multiple change of shear activity between elements of a conjugate system appears coherent with a far-stress regime as established in the experiments. We found no indications of simultaneous activity of both conjugate sets in any of our experiments.

2.4.3. Course of the interaction process

The experimental results suggest the following steps of an interaction process (Figs. 11, 12; internal rotation effects have been omitted):

(a) At some distance from fault 1, a conjugate fault 2 grows towards fault 1. Example: Fig. 5a.
(b) Fault 2 becomes highly active and approaches fault 1. Examples: Fig. 8a,b.
(c) Fault 2 tip becomes increasingly deflected far outside the shear zone of fault 1. Example: Fig. 6a.
(d) Fault 2 has merged into the dominant fault 1 forming a confluence bow. During this process, it doesn't change its shear sense until entering the shear zone of fault 1. Examples: Figs. 1A, 5b,c, 6b,c, 8c, 13A,B.
(e) Change of the shear activity to fault 2 and formation of a confluence branch at the point of beginning deflection. The branch is growing straight ahead disregarding the curved section. Examples: Figs. 1B,C, 5d, 8d,e, 9, 13C,D.
(f) Intersection and displacement of fault 1 by propagation of the confluence branch of fault 2. Examples: Figs. 5e, 6d,e, 8f, 10, 13E.
(g) Reactivation of the fault 1 segments: fault 2 now becomes dissected by the formation of linkage faults enabling slip over the step of fault 1. This indicates another change of shear activity. Example: Fig. 8g.
(h) Displacement of fault 2 along the linkage faults. Example: Fig. 8h.
(i) Another reactivation of the fault 2 segments leads to a further system of linkage faults. Examples: Fig. 8i,j.
(j) A complex pattern has been produced in the intersection area enabling other mechanisms, such as block rotation, to become active rather than forming further intersection blocks.

3. Discussion

3.1. Outline of a supplemented conjugate fault concept

Since Daubrée's experiments (Daubrée, 1878), conjugate faults have been well known elements of faulting processes. An important restriction of most of the current shear models relates to their focus on the problem of a single fault or shear zone. Conjugate systems, however, consist of two sets of shear planes with different orientation and kinematic functions. According to the Coulomb shear

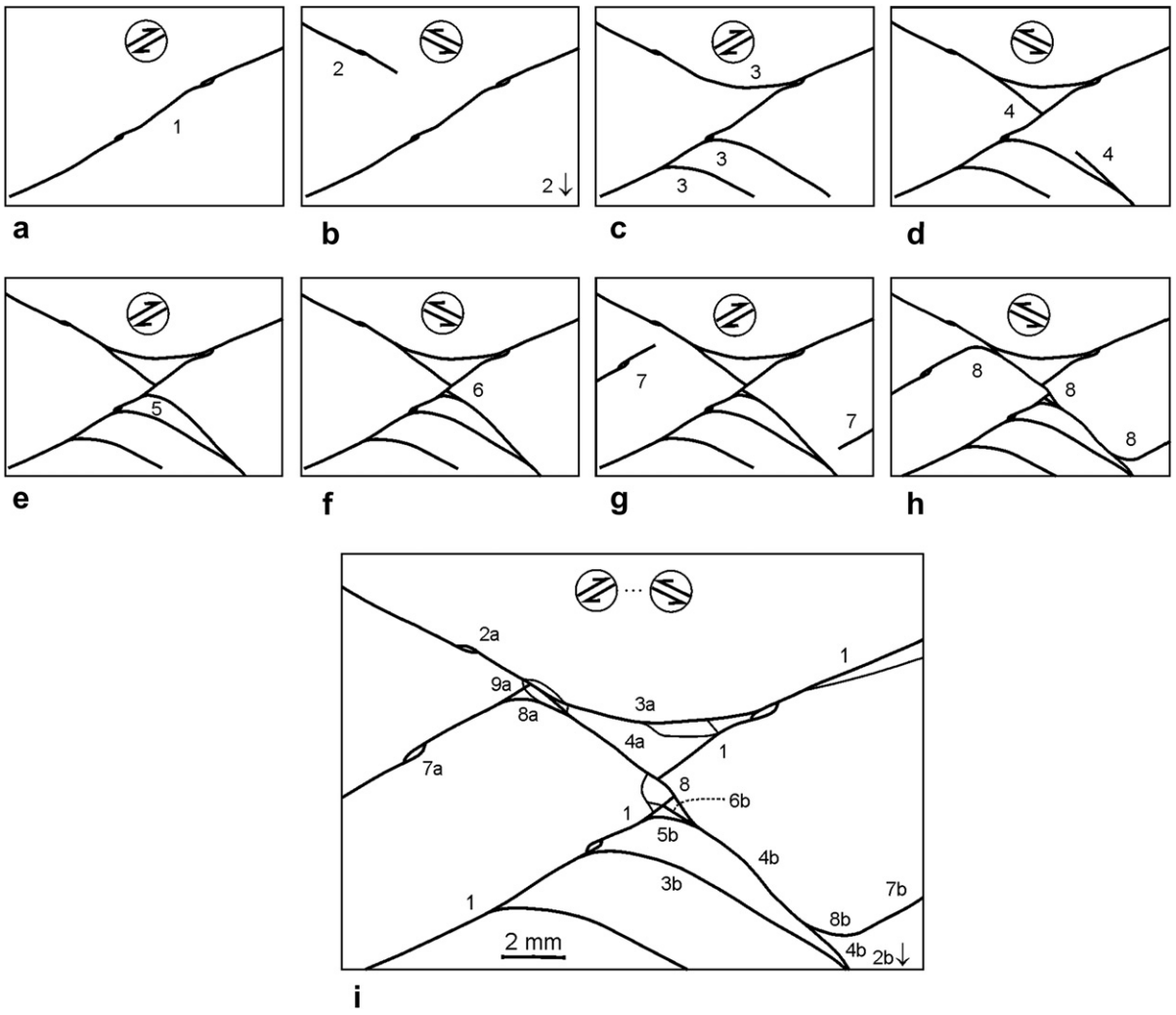

Fig. 11. Reconstruction of the structural evolution of the intersection pattern of Fig. 10. Stages a–h denote phases of dextral or sinistral shear sense regimes indicated by encircled arrows. Stage i shows the detailed fault pattern of Fig. 10 and comprises two further shear sense regimes. Numbers indicate the succession of fault generation and activity. Corresponding faults on either side of primary fault 1 are marked by letters a and b (only for stage i). Some secondary faults (thin lines on stage i) have been omitted in the stage series. The final fault displacing fault 1 is considered a joint fault composed of the elements 2a–4a–8–4b–2b. The central fault element 8 is considered a linkage fault.

criterion, it is not known whether only the dextral or sinistral fault or both of them will be generated under the critical stress. Local material properties will ultimately be decisive.

The rheological behaviour of the clay material disclosed an initial very short interval of elastic strain followed by a ductile strain period, during which domains of deformation bands develop. These domains appeared to be organized like conjugate fault sets. At some sites, indications of overprinting of each other were observed. This is suggestive of a change of activity within these domains. Single faults slowly develop parallel to a set of active deformation bands. This is considered a transition period to brittle strain behaviour. Later on, brittle strain is clearly expressed by mode 1 distal splays at fault terminations or the formation of fissures and small gaps along faults.

The model of confluence and intersection is based on the confluence bow and the alternating activity of growth and shear of conjugate faults. They have to be integrated into the dynamic system of conjugate faults. Some crucial features appear to be indicative for the confluence mechanism: (1) pre-existing conjugate shear conditions, (2) deflection towards the obtuse angle side of the conjugate elements or, in other words: curving right of dextral faults and vice versa, (3) the distance of the point of starting deflection to the conjugate fault (defining a deflection zone parallel to it) is considerably greater than its shear zone width, and (4) the occurrence at an early stage of the interaction process, i.e. propagation of the curving fault only into still unfaulted areas prior to the intersection stages.

When summarizing these points, we have to consider the transition period from ductile to brittle strain as relevant for the fault deflection. This means an interaction of a deformation band field and a conjugate fault 2 propagating directly into that field. This field is situated in front of fault 1 and displays coherent behaviour. However, the details of these microscopic processes within the deflection zone have not yet been precisely examined. According to observations on markers, the resulting deflected fault 2 doesn't change its sense of shear until entering the shear zone of fault 1, where its shear activity dominates that of the merging fault.

Due to the late occurrence of splay faults, typical for brittle strain behaviour, we did not see them exert any decisive influence on the deflection process, despite the fact that they occur at similar positions as the confluence bows. Instead thereof, all indications point to an involvement of ductile strain processes rather than to pure brittle strain behaviour. The latter, on the other hand, characterizes the intersection stages.

Whereas the processes within the deflection zone need to be further investigated, many details are available on the macroscopic

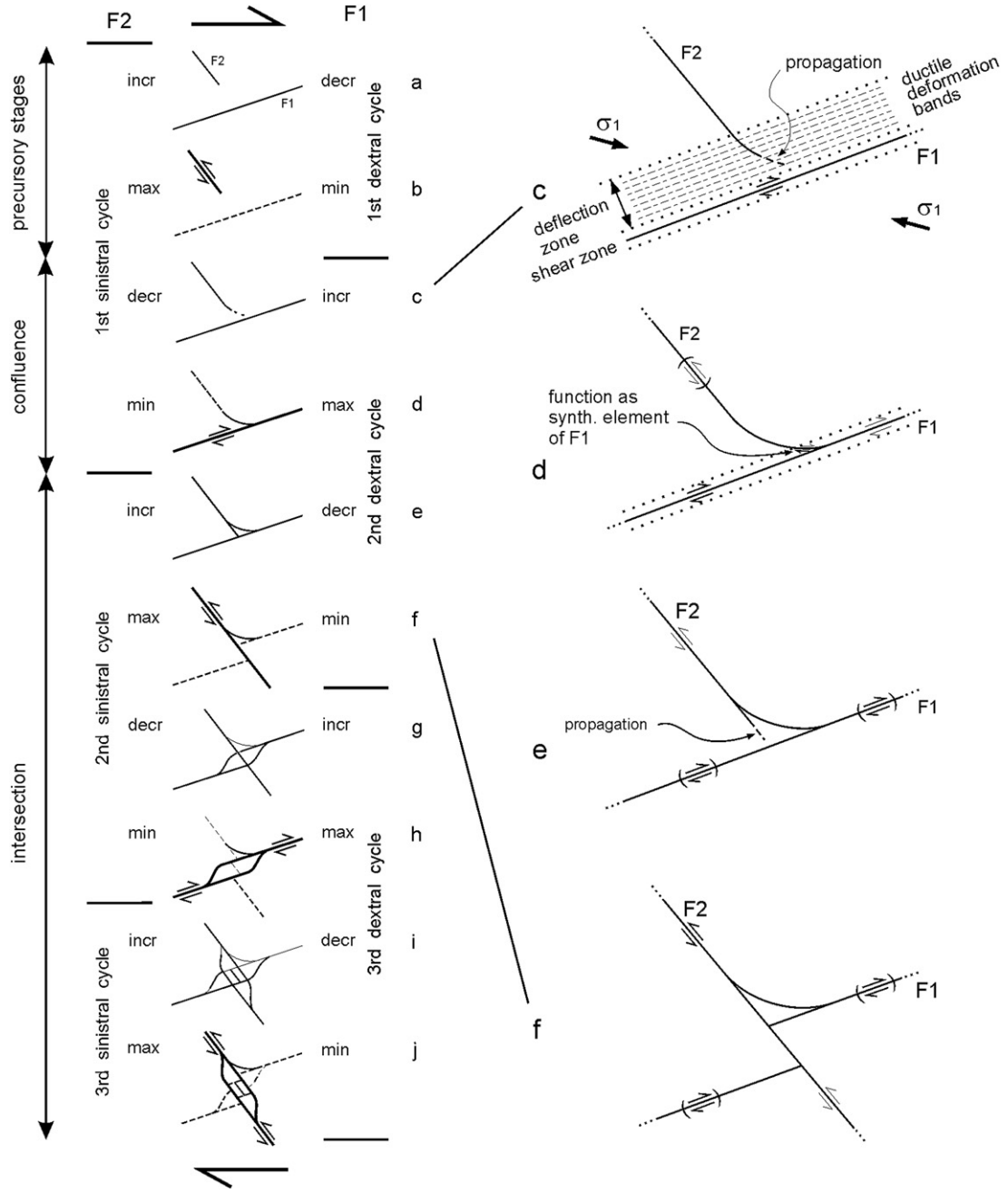

Fig. 12. Scheme of the evolution of a dextral conjugate fault system and its activity cycles along dextral (F1) and sinistral (F2) fault elements. Dextral and sinistral cycles are defined by four activity levels which correspond to fault line styles: incr, increasing; max, maximum; decr, decreasing; min, minimum. Bold lines: dominant faults. Enlarged stages set focus on the development of the confluence bow (c, d) and beginning intersection (e, f). Late cycle stages (g–j) are characterized by additional linkage faults.

structural evolution. They suggest some additions on the kinematic scheme of conjugate faults as outlined in Fig. 12. The observations of alternating fault activity concerning propagation and shearing led us to a system of dextral and sinistral activity cycles for the conjugate fault sets.

The experimental indications of long and short activity cycles of the interacting faults (Section 2.4.2) fit well into existing models of displacement and earthquake cycles based on shear stress and strain accumulation followed by relaxation (Turcotte and Schubert, 1982, p. 367–373; Thatcher, 1990; Cowie and Scholz, 1992; Manzocchi et al., 2006). Whereas most of those models consider the single fault problem, only a few examples exist for conjugate fault systems with a multiple change of activity (e.g. Lamouroux et al., 1991; Olsson et al., 2004). Nicholson et al. (1986) provided data from the San Andreas system on alternating seismic activity between the main fault zones (San Andreas F.Z. and San Jacinto F.Z.) and new antithetic elements in between.

The introduction of the confluence bow as new fault element has to be distinguished from other curved fractures such as curved joints (Dyer, 1988; Engelder and Gross, 1993), listric faults, and drag of dissected non-conjugate faults. However, none of these structures fits the specific features of confluence bows or presents a confluence branch.

Some conditions generally responsible for structural complications have been neutralized or excluded from the experiments, such as effects due to inhomogeneity, anisotropy and additional stress regimes. Strong internal fault rotation determines the end of shearing along a fault section and the beginning of its passive

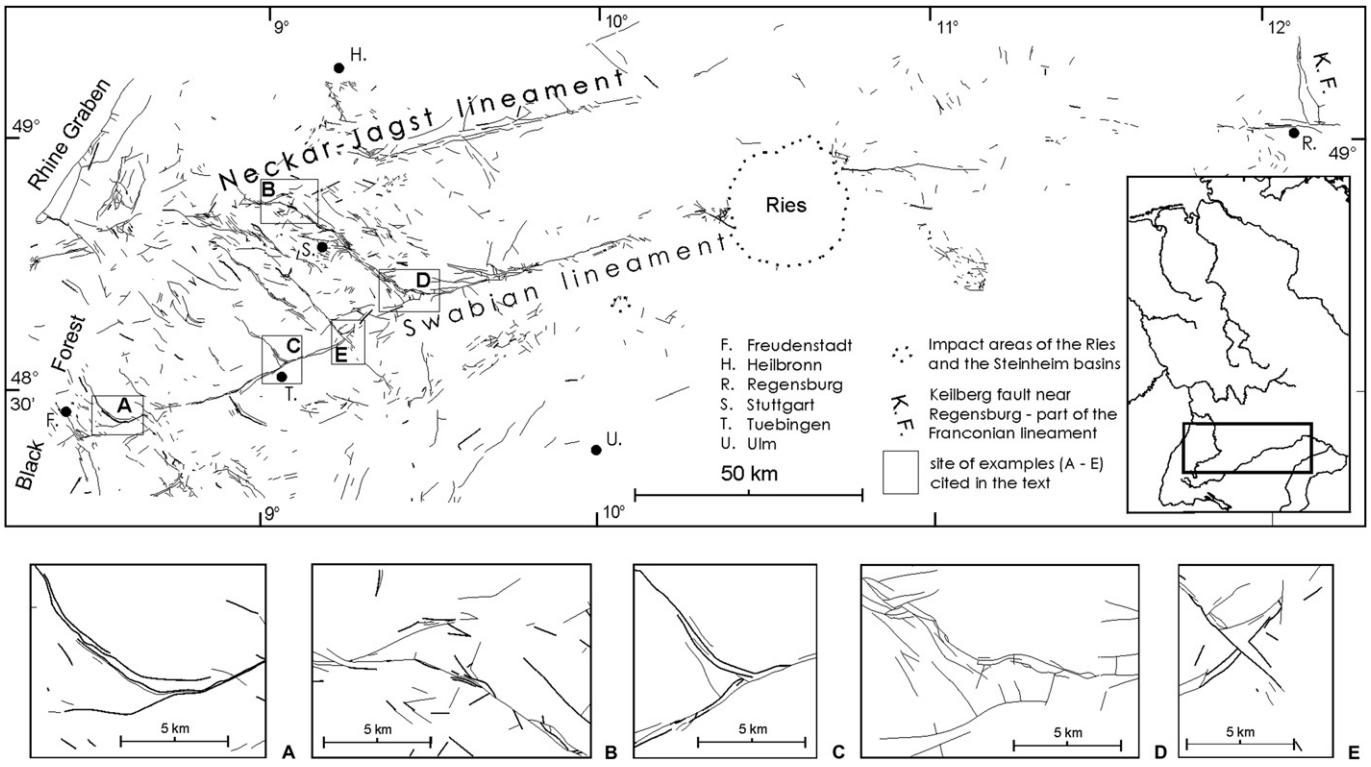

Fig. 13. The Swabian fault system as the most characteristic structural feature of southern Germany between the Black Forest and the Franconian lineament (represented by the sub-element of the Keilberg fault, K.F.) is dominated by the Swabian lineament in the south and the Neckar–Jagst lineament in the north. Both lineaments are connected by NW–SE trending conjugate fault zones, which generally bend into the bordering lineaments on either end. Compiled from survey map series of various scales. Example boxes: A, B: confluence structures; C–E: various stages of intersection structures.

deformation. Growth of the rotated faults produces new segments at both ends according to the unchanged stress direction. This results in differently curved faults subject to the type of deformation (pure shear or simple shear; Hoeppener et al., 1978) and fault character (synthetic or antithetic). All rotational effects, excluding rotated antithetic faults, produce curved segments towards the reversed direction of confluence bows. Furthermore, confluence is restricted to early stages of interaction, whereas internal rotation effects become obvious at late stages.

3.2. Natural examples

Comparison of experimental fabrics with natural occurrences is usually restricted to geometric similarity. Studies using full dynamic similarity are generally based on Reynolds numbers, which often have an insufficient database on the natural objects or address very spacious objects such as crustal structures. However, by focusing on only the type of fabric, its symmetry, and the phenomenological evolution of structural patterns, and not on spatial and temporal dimensions, we are relatively free to design the experiments so that we obtain those structures one finds in nature. In our case, the geometric similarity of all experimental stages to natural occurrences was so great that we excluded simple coincidence or convergence of the phenotypes. All natural examples of confluence structures found in the literature, excluding those of Anderson (1951), are merely documented by maps, photographs or drawings and not described or specifically discussed. Instead of implying dynamic similarity, we present a few natural examples only to demonstrate the variety of patterns and ubiquity and to stimulate further investigations.

Swabian fault system: Trending from WSW to ENE over a distance of about 280 km through southern Germany from the eastern margin of the Black Forest near Freudenstadt to the western margin of the southern Bavarian Forest near Regensburg. Especially in its western section, it reveals a conjugate fault pattern including many varieties of the confluence and intersection structures we observed in the experiments (Fig. 13, example boxes A–E). Under "Swabian fault system" we understand two confining large fault zones, the Swabian lineament in the south (Seibold, 1951; Carlé, 1955) and the Neckar–Jagst lineament in the north (Dürr, 1982), which include many fault zones in between, such as the Fildergraben around Stuttgart (Carlé, 1955). Three different patterns schematically depicted in Fig. 2 are recognized: (1) simple confluence bows of NW–SE striking fault zones merging into the southern master fault zone (type Fig. 2b), e.g. E of Freudenstadt (Fig. 13A), or merging into the northern master fault zone, e.g. near Schwieberdingen NW of Stuttgart (Fig. 13B); (2) confluence bows with branches (type Fig. 2c), e.g. near Tuebingen (Fig. 13C) or near Plochingen SE of Stuttgart (Fig. 13D); (3) intersection patterns of NW–SE striking faults dissecting the Swabian lineament faults with some offset (type Fig. 2d), e.g. near Aichtal S of Stuttgart (Fig. 13E).

Drevenacker Fault: Trending WNW–ESE over a length of about 25 km through the north-western Ruhr district (western Germany; Fig. 1), both a dextral strike-slip and a northern dip-slip component have been recognized (Wolf, 1988). Displacement activities during Upper Carboniferous, Permian–Triassic, Tertiary, and Quaternary have been recognized as well as an Upper Cretaceous inversion (Wrede and Jansen, 1993; Wrede, 2000). On its southern side, three NNW–SSE striking conjugate faults—KBV fault (Fig. 1A), Krudenburg fault (Fig. 1B), Huenxe fault (farther west outside the map)—run into the Drevenacker fault with a distinct right bending confluence bow (type Fig. 2b), whereas on its northern side a yet unnamed conjugate fault (Fig. 1C) displays a left bending confluence bow

including a confluence branch (type Fig. 2c). The latter type is also developed at the Krudenburg fault (Fig. 1B).

Southern Upland Fault System SE of Ayr/southern Scotland: Anderson, 1951, p. 53–55, (figure 17) published a detailed description of a double-sided confluence at the Southern Upland Fault, where two left bending conjugate faults on its northern side and two right bending fault segments on its southern side merge into the master fault (type Fig. 2b). Although no shear sense of the faults has been determined, Anderson supposed a simple displacement (Anderson, 1951, p. 54: "The two dykes are thus deflected some 20 km out of their previous alignment.") The double-sided confluence was obviously interpreted as a drag phenomenon. According to our model exactly the opposite shear sense appears to be appropriate.

Scottish Central Coalfield: In the classical book by Anderson, 1951, p. 31–33, (figures 10 and 11), there is also a well-founded written documentation illustrated with maps and diagrams, which could serve as paradigm for a conjugate fault system. The area between Hamilton and Wishaw SE of Glasgow displays a classical parquet pattern of a pure shear conjugate fault system with confluence bows in the obtuse angle position, often completed by a confluence branch (types Fig. 2b and c).

From the vast variety of examples found in the literature only two meso-scale confluence structures are cited here: (1) type Fig. 2b structure in Navajo Sandstone of the Colorado Plateau (Bump and Davis, 2003, Fig. 6F) and (2) type Fig. 2b and c structure in Tertiary limestones of Gozo Island, Malta (Kim et al., 2003, Figs. 5 and 9).

4. Conclusions

The answer to the initial question concerning the behaviour of interacting conjugate faults led to the concept of confluence and intersection. It comprises the entire period of shear-dominated activities along conjugate faults.

The introduction of the new term "confluence" is convenient to characterize the significant shape of the curved link between conjugate faults and the specific conditions of its occurrence. Evidence of alternating shear activities at the fault sets and the resulting intersection patterns define the main interaction phase, designated by the known term "intersection".

The feature of confluence widens the focus from crossing faults to strain processes around fault planes, and provides a new incentive for better understanding of the rheology of shear processes. Indications of interacting deformation bands prior to the occurrence of faults are a reason for the inclusion of the early stage of ductile strain as well as multiple intersection stages into the entire process as long as shearing along the conjugate faults and its precursors is governed by the same remote stress field. The deflection of a fault propagating into a domain of active deformation bands indicates an interaction stage of ductile and brittle strain behaviour. This is considered a transition period to pure brittle strain. Generally, the intersection of conjugate faults will end with the formation of linkage faults. Further interaction structures, such as irregular fragmentation in the interaction region, are primarily due to block rotation effects rather than to shear processes.

The specific geometric and kinematic features of confluence and intersection structures support the reconstruction of interaction processes and the recognition of the stage of the structural evolution. Especially the confluence bow may prove to be a valuable tool for the shear sense of a juvenile fault system. A comprehensive analysis of natural examples might yield insight into possible applications of the proposed concept. A first comparison with natural examples did not reveal any principal structural differences from the scheme based on the laboratory results.

Acknowledgements

An early stage of this research project was funded by the Deutsche Forschungsgemeinschaft (Schw 238/3-1). The authors would like to thank Beatrix Haglauer-Ruppel for close cooperation in the lab and discussions on early results. We are greatly indebted to many unnamed students for their help with the laboratory experiments. Attila Aydin, Andrea Billi, Terry Engelder, Reinhard Hesse and three anonymous reviewers contributed valuable improvements to the manuscript, which is greatly acknowledged.

References

Anderson, E., 1951. The Dynamiques of Faulting and Dyke Formation with Applications to Britain, second revised ed. Oliver & Boyd, Edinburgh.
Bump, A.P., Davis, G.H., 2003. Late Cretaceous-early Tertiary Laramide deformation of the northern Colorado Plateau, Utah and Colorado. Journal of Structural Geology 25, 421–440.
Carlé, W., 1955. Bau und Entwicklung der Südwestdeutschen Großscholle. Beihefte zum Geologischen Jahrbuch 16.
Cowie, P.A., Scholz, C.H., 1992. Growth of faults by accumulation of seismic slip. Journal of Geophysical Research 97, 11085–11095.
Daubrée, G., 1878. Recherches expérimentales sur les cassures qui traversent l'écorce terrestre, particulièrement celles qui sont connu sous les noms de joints et failles. Academie des Sciences Comptes Rendus 86, 77–83.
Davatzes, N.C., Aydin, A., 2003. The formation of conjugate normal fault systems in folded sandstone by sequential jointing and shearing, Waterpocket monocline, Utah. Journal of Geophysical Research 108, ETG 7, 1–15.
Dürr, R., 1982. Strukturgeologische Untersuchungen im Bereich der Neckar-Jagst-Furche (Baden-Württemberg). Arbeiten des Instituts für Geologie und Paläontologie der Universität Stuttgart, Neue Folge. 77, 75–146.
Dyer, R., 1988. Using joint interactions to estimate paleostress ratios. Journal of Structural Geology 10, 685–699.
Engelder, T., Gross, M.R., 1993. Curving cross joints and the lithospheric stress field in eastern North America. Geology 21, 817–820.
Ferrill, D.A., Morris, A.P., Stamatakos, J.A., Sims, D.W., 2000. Crossing conjugate normal faults. American Association of Petroleum Geologists Bulletin 84, 1543–1559.
Flodin, E.A., Aydin, A., 2004. Evolution of a strike-slip fault network, Valley of Fire State Park, southern Nevada. Geological Society of America Bulletin 116, 42–59.
Hoeppener, R., Schwarz, H.-U., 1980. Experimentelle Untersuchungen über Schiefergefüge und Gefüge in geschieferten Gesteinsverbänden. Neues Jahrbuch für Geologie und Paläontologie Abhandlungen 160, 363–379.
Hoeppener, R., Kalthoff, E., Schrader, P., 1969. Zur physikalischen Tektonik. Bruchbildung bei verschiedenen affinen Deformationen im Experiment. Geologische Rundschau 59, 179–193.
Hoeppener, R., Kalthoff, E., Schrader, P., 1968. Experimentelle Untersuchungen über Bruchbildung. Bergbauwissenschaften 16, 174–177.
Hoeppener, R., mit Beiträgen von Mischke, H., Schäfer, G., Schwarz, H.-U., 1978. Grenzen quantitativer Untersuchungen bei tektonischen Experimenten. Geologische Rundschau 67, 858–879.
Horsfield, W., 1980. Contemporaneous movement along crossing conjugate normal faults. Journal of Structural Geology 2, 305–310.
Kalthoff, E., 1970. Bruchbildung in Modellsubstanzen bei Deformationen mit axialer und rhombischer Symmetrie. Dissertation, University of Bochum.
Kim, Y.-S., Peacock, D., Sanderson, D.J., 2003. Mesoscale strike-slip faults and damage zones at Marsalforn, Gozo Island, Malta. Journal of Structural Geology 25, 793–812.
Lamouroux, C., Ingles, J., Debat, P., 1991. Conjugate ductile shear zones. Tectonophysics 185, 309–323.
Manzocchi, T., Walsh, J.J., Nicol, A., 2006. Displacement accumulation from earthquakes on isolated normal faults. Journal of Structural Geology 28, 1685–1693.
Nicholson, C., Seeber, L., Williams, P., Sykes, L.R., 1986. Seismic evidence for conjugate slip and block rotation within the San Andreas fault system, Southern California. Tectonics 5, 629–648.
Nicol, A., Walsh, J.J., Watterson, J., Bretan, P., 1995. Three-dimensional geometry and growth of conjugate normal faults. Journal of Structural Geology 17, 847–862.
Olsson, W., Lorenz, J.C., Cooper, S.P., 2004. A mechanical model for multiply-oriented conjugate deformation bands. Journal of Structural Geology 26, 325–338.
Reches, Z., 1988. Evolution of fault patterns in clay experiments. Tectonophysics 145, 141–156.
Schrader, P., 1970. Bruchbildung in Modellsubstanzen durch Deformationen mit monokliner Symmetrie. Dissertation, University of Bochum.
Seibold, E., 1951. Das Schwäbische Lineament zwischen Fildergraben und Ries. Neues Jahrbuch für Geologie und Paläontologie Abhandlungen 93, 285–324.
Thatcher, W., 1990. Present-day crustal movements and the mechanics of cyclic deformation. U.S. Geological Survey Professional Paper 1515, 189–205.
Tikoff, B., Wojtal, S.F., 1999. Displacement control of geologic structures. Journal of Structural Geology 21, 959–967.

Turcotte, D.L., Schubert, G., 1982. Geodynamics. Application of Continuum Physics to Geological Problems. Wiley & Sons, New York.
Watterson, J., Nicol, A., Walsh, J., Meier, D., 1998. Strains at the intersections of synchronous conjugate normal faults. Journal of Structural Geology 20, 363–370.
Weber, K., 1976. Gefügeuntersuchungen an transversalgeschieferten Gesteinen aus dem östlichen Rheinischen Schiefergebirge. (Ein Beitrag zur Genese der transversalen Schieferung). Geologisches Jahrbuch D15, 3–98.
Wolf, R., 1988. Tiefentektonik des Dorstener Hauptsattels zwischen Rheinberg und Dorsten im westlichen Ruhrgebiet. In: Kunz, E., Wolf, R., Wrede, V. (Eds.), Ergänzende Beiträge zur Tiefen tektonik des Ruhrkarbons. Geologisches Landesamt Nordrhein-Westfalen, Krefeld, pp. 9–33.
Wrede, V., 2000. Erläuterungen zu Blatt 4407 Bottrop. Geologische Karte von Nordrhein-Westfalen 1:25000, second ed.
Wrede, V., Jansen, F., 1993. Nachweis quartärzeitlicher Bruchtektonik im Ruhrgebiet. Neues Jahrbuch für Geologie und Paläontologie Monatshefte 1993, 733–748.